Letter

Luminescence properties of dislocations in α-Ga$_2$O$_3$

Mugove Maruzane[1,*] , **Yuichi Oshima**[2] , **Olha Makydonska**[1] , **Paul R Edwards**[1] ,
Robert W Martin[1] **and Fabien C-P Massabuau**[1]

[1] Department of Physics, SUPA, University of Strathclyde, Glasgow, United Kingdom
[2] National Institute for Materials Science, Tsukuba, Japan

E-mail: mugove.maruzane@strath.ac.uk

CrossMark

Abstract

Dislocations in epitaxial lateral overgrown α-Ga$_2$O$_3$ are investigated using hyperspectral cathodoluminescence spectroscopy. The dislocations are associated with a reduction of self-trapped hole-related luminescence (*ca.* 3.6 eV line) which can be ascribed to their actions as non-radiative recombination sites for free electrons, to a reduction in free electron density due to Fermi level pinning or to electron trapping at donor states. An increase in the intensity of the *ca.* 2.8 eV and 3.2 eV lines are observed at the dislocations, suggesting an increase in donor–acceptor pair transitions and providing strong evidence that point defects segregate at dislocations.

Supplementary material for this article is available online

1. Introduction

Wide bandgap semiconductors offer exciting perspectives for the fabrication of high-power and high-frequency electronic devices, as illustrated by their high Baliga and Johnson figures of merit [1, 2]. One such wide bandgap semiconductor is Ga$_2$O$_3$ which can form five polymorphs, labelled α, β, γ, κ and δ [3, 4]. Monoclinic β-Ga$_2$O$_3$ is the most studied phase of Ga$_2$O$_3$ due to its thermal stability, but corundum α-Ga$_2$O$_3$ has been gaining popularity recently due to its wider bandgap in the range of 5.1–5.3 eV [5, 6] and its promise of

bandgap engineering through alloying with other corundum sesquioxides [7–12]. However, unlike β-Ga$_2$O$_3$ which can be grown from the melt, the metastable nature of α-Ga$_2$O$_3$ means that it can only be produced by epitaxial methods such as halide vapour phase epitaxy [13–15], molecular beam epitaxy [16–19], metal-organic chemical vapour deposition [17, 20], mist chemical vapour deposition [5, 21, 22] and atomic layer deposition [6, 23, 24]. α-Ga$_2$O$_3$ is usually grown on isomorphic sapphire (α-Al$_2$O$_3$) substrates; however, the 4.7% and 3.3% lattice mismatch between the film and the substrate in the *a* and *c* directions, respectively, results in a high density of threading dislocations of *ca.* 10^{10}cm^{-2} [5, 14].

The effects of dislocations on the properties of any polymorph of Ga$_2$O$_3$ are poorly understood. Kasu *et al* [25] reported that dislocations resulted in higher reverse leakage currents in β-Ga$_2$O$_3$ [25], and Yang *et al* [26] stated that crystal defects (including dislocations) can explain the reason why the theoretical rectifying limit for β-Ga$_2$O$_3$ has not yet been attained [26]. In α-Ga$_2$O$_3$, dislocations have been linked to reduced

* Author to whom any correspondence should be addressed.

J. Phys. D: Appl. Phys. **58** (2025) 03LT02

Letters

electron mobility [27, 28]. The anticipated negative impact of dislocations has triggered research into the design of methods to mitigate their occurrence. A promising method currently employed for α-Ga_2O_3 is epitaxial lateral overgrowth (ELOG) [29–33] which allows the reduction of threading dislocation density from *ca.* $10^{10} cm^{-2}$ to *ca.* $10^6 cm^{-2}$ [29, 31–33]. Despite these efforts to reduce dislocation densities, it is also important to understand their properties to predict their impact on future device performance and design effective strategies to mitigate their effects.

Cathodoluminescence (CL) is a powerful technique used to probe the optical properties of semiconductors with nanoscale resolution and correlate these with the presence of defects [34]. The method has been successfully used to reveal the optical properties of dislocations in other wide bandgap semiconductors like III-nitrides [35–37] but has not yet been employed for studying dislocations in α-Ga_2O_3.

The luminescence spectrum of α-Ga_2O_3 (as well as β-Ga_2O_3) is characteristically broad [38–42]. Luminescence spectra generally do not contain a near-band edge contribution close to 5 eV [38, 40–43], and instead, the luminescence spans from *ca.* 2.0–3.8 eV [38, 41]. Nicol *et al* [41] reported H-related luminescence in α-Ga_2O_3 at 3.8 eV [41]. UV luminescence near *ca.* 3.2–3.6 eV has been ascribed to the recombination of self-trapped holes with free electrons [38–40, 42, 44–46]. Blue luminescence in the range of *ca.* 2.8–3.0 eV, has been ascribed to donor–acceptor pair transitions between shallow donors and acceptors involving gallium or oxygen vacancies [38, 46–50]. Green luminescence observed in the range 2.0–2.7 eV has been ascribed to donor–acceptor pair transitions between deep donors and acceptors, usually formed from complexes of oxygen vacancies, gallium vacancies, gallium interstitials and oxygen interstitials [45, 51, 52]. Finally, red luminescence at *ca.* 1.7–1.9 eV, has been observed in β-Ga_2O_3 but has yet to be observed in α-Ga_2O_3. In β-Ga_2O_3, red luminescence has been linked to the presence of dopants such as nitrogen, chromium and silicon [45, 53–56]. The effect of extended defects on the luminescence properties in Ga_2O_3 polymorphs has not been widely discussed. Cooke *et al* [57] assessed the effect of extended defects on the photoluminescence spectra of β-Ga_2O_3 films grown on different substrates, which resulted in a variation of strain and, by extension, a variation of extended defect density. In that study, extended defects were linked to a decrease in intensity and a redshift of the luminescence [57]. In the present report, we investigate how threading dislocations affect the CL spectrum of ELOG α-Ga_2O_3 with a nanoscale resolution.

2. Experimental methods

We investigated the luminescence properties of dislocations in an ELOG α-Ga_2O_3 sample grown using halide vapour phase epitaxy (HVPE) on *c*-plane sapphire following the ELOG recipe detailed by Oshima *et al* [29]. After the growth of an initial α-Ga_2O_3 seed layer, a TiO_2 mask consisting of 5 μm wide stripes separated by 1 μm wide windows was deposited

with stripes oriented parallel to [1$\bar{1}$00]. This was followed by the deposition of a *ca.* 21 μm layer of α-Ga_2O_3. Finally, the sample surface was etched using HCl gas to reveal pits indicating where threading dislocations, in particular edge-type, terminate at the sample surface [33].

Secondary electron (SE) and hyperspectral CL imaging were conducted using a JEOL JXA-8530F field emission electron probe micro-analyser (EPMA). The microscope was operated with an acceleration voltage of 8 kV and a beam current of 5 nA, resulting in an interaction volume size of *ca.* 240 nm based on Monte Carlo simulations [58]. The luminescence was collected at room temperature using a reflecting objective and was directly coupled to a cooled CCD spectrograph, allowing a CL spectrum to be recorded for each pixel in the scan. The resulting CL spectra were corrected for system response using the transition radiation of pure aluminium [59].

3. Results and discussions

Figure 1(a) shows an SE image of the sample surface. The window (1 μm wide) and mask (5 μm wide) regions can be easily identified as regions with high and low densities of etch pits, respectively. At the centre of the mask region, where the α-Ga_2O_3 coalesces, is a thin line of lightly packed etch pits that also runs parallel to the window regions (i.e. [1$\bar{1}$00]) as reported by Oshima *et al* [33]. Figure 1(b) shows the corresponding panchromatic CL image (photon energies in the range of 1.5–5 eV) showing the integrated CL intensity recorded at each pixel. These maps show that the positions of the etch pits in the SE image seem to correlate with reduced CL luminescence. More importantly, the map also reveals additional dark contrast lines oriented along the $\langle 1\bar{1}00 \rangle$ directions which propagate from the window region to the etch pits. Kawara *et al* [31] previously reported, in dot-patterned ELOG α-Ga_2O_3, that dislocations could bend from the window region into the masked region following the $\langle 1\bar{1}00 \rangle$ direction [31]. These studies also observed that the dislocations which bend deep within the film would terminate at the coalescence boundary [29, 31]. Such dislocations would therefore not cause an etch pit at the sample surface, and their bent section would occur too deep in the sample for the electron beam to probe. This strongly suggests that the dark contrast lines in our panchromatic CL map relate to dislocations bending sufficiently close the sample surface (i.e. within the 240 nm depth probed by the electron beam) from the window region and terminating at etch pits in the mask region.

To start assessing how dislocations affect the luminescence properties of α-Ga_2O_3, we first look at CL spectra taken away from a dislocation line (figure 1(c)) and at a dislocation line (figure 1(d)). Both spectra align with the literature on α- and β-Ga_2O_3 luminescence, and can be well fitted using 3 Gaussian peaks in agreement with other examples of luminescence spectra from the literature [40, 41, 45]. We observe a first peak (labelled 'Peak 1') centred at *ca.* 3.6 eV and attributed to self-trapped holes, as well as a second and third peak ('Peak

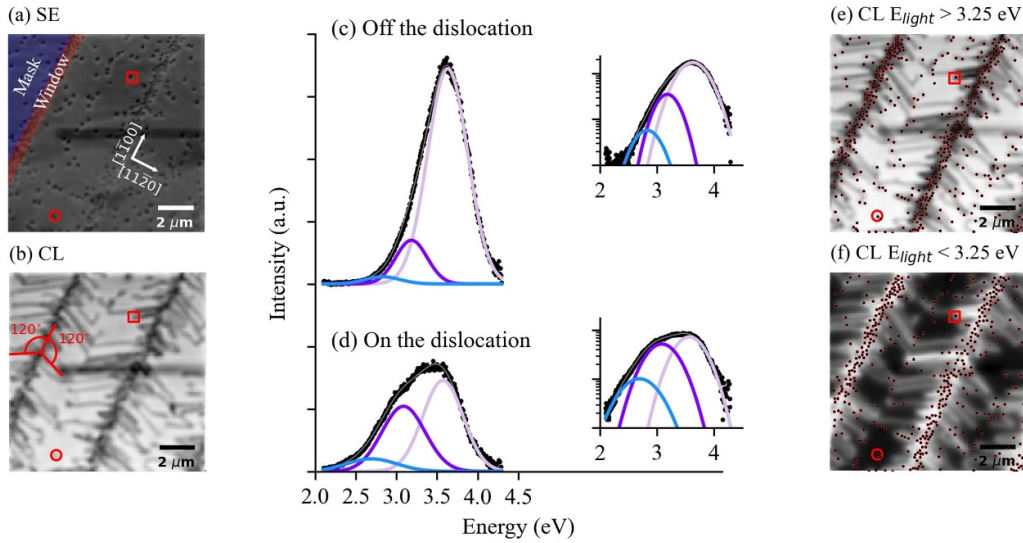J. Phys. D: Appl. Phys. **58** (2025) 03LT02

Letters

Figure 1. (a) SE and (b) panchromatic CL maps of the same area of the sample. Example CL spectra taken on a pixel (c) away from dislocations, and (d) at a dislocation. Bandpass-integrated CL maps for emission energies (e) above 3.25 eV and (f) below 3.25 eV. To guide the eye, the positions of etch pits identified from the SE image were manually marked by dots in (e) and (f). An example of an etch pit linked (not linked) to a dislocation line is highlighted by a square (circle) box.

2' and 'Peak 3') centred at *ca.* 3.2 eV and 2.8 eV, respectively, attributed to donor–acceptor pair transitions [38, 40, 42]. We can already observe differences depending on the position relative to the dislocation, where the CL spectrum taken at the dislocation exhibits an overall weaker and redshifted luminescence compared to that of the region away from the dislocation—we analyse these variations in more detail in the next section. Figures 1(e) and (f) show bandpass-integrated CL maps of the sample extracted from the hyperspectral CL map, discriminating emission of photons >3.25 eV (i.e. dominant contribution from Peak 1, figure 1(e)) from emission of photons <3.25 eV (i.e. dominant contribution from Peaks 2 and 3, figure 1(f)). To guide the eye, red-bordered dots are used to indicate the locations of the etch pits. These two maps show a contrast inversion, where the dislocation lines appear dark in the map for emission >3.25 eV (figure 1(e)) and bright in the map for emission <3.25 eV (figure 1(f)), in line with our observation of individual CL spectra (figures 1(c) and (d)).

Further investigation identifies two different categories of etch pits. The first category corresponds to pits connected to a dislocation line in the CL map (an example of which is marked by a square in figure 1), while the second category corresponds to pits that are not linked to a dislocation line in the CL map (an example of which is marked by a circle in figure 1). We calculated a density of etch pits of *ca.* 1.5×10^6 cm^{-2} in the mask region, which is in line with the value reported by Oshima *et al* [33], and we estimate that *ca.* 85% of etch pits fall into the first category of pits, with the remainder *ca.* 15% falling into the second category.

To better understand the luminescence properties of the dislocations, we acquired a linescan to investigate the evolution of the luminescence spectrum as the electron probe scans across dislocation lines, shown in figure 2. While we note that the dislocation line and the etch pit terminating it exhibit the same

luminescence, analysing the dislocation line, which is a sub-surface feature, allows us to rule out the potential impact of the HCl etching on the CL data. As discussed previously, each CL spectra was fitted using 3 Gaussian peaks, and the evolution of the integrated intensity and energy of each Gaussian peak was monitored across the linescan (figures 2(d) and (e)). The deconvolution of each individual spectrum from the linescan is shown in the supplementary information (figure S1).

The first peak, centred at *ca.* 3.6 eV can be seen to vary significantly across the linescan. We observe that compared to the region away from the dislocation, the intensity decreases by a factor *ca.* 2 at the dislocation and redshifts by *ca.* 0.04 eV. This luminescence line is commonly ascribed to radiative recombination of free electrons with self-trapped holes [38, 40, 42, 44–46, 60]. Given that self-trapped holes are strongly localised at O sites [45], it is reasonable to interpret this decrease in intensity as a reduction of the density of free electrons, which would therefore be involved in competing recombination pathways near the dislocation. One interpretation could be that these electrons get more efficiently trapped at donor states. If this was the case, we should expect to see an increase in donor–acceptor pair transitions at dislocations, which we observe to some extent with variations of Peaks 2 and 3. However, that increase in donor–acceptor pair transition does not compensate for the reduction of Peak 1 luminescence, suggesting an additional recombination pathway is at play. The reduction of free electron recombination with self-trapped holes could also be caused by an increase in non-radiative recombination at the dislocation, as has been widely observed in other semiconductors [35, 61, 62]. One last interpretation could be that the electrons drift away from the dislocation region due to Fermi level pinning at the dislocation, for example, because of a charged dislocation core [63]. A comprehensive assessment of the correct interpretation necessitates knowledge of the
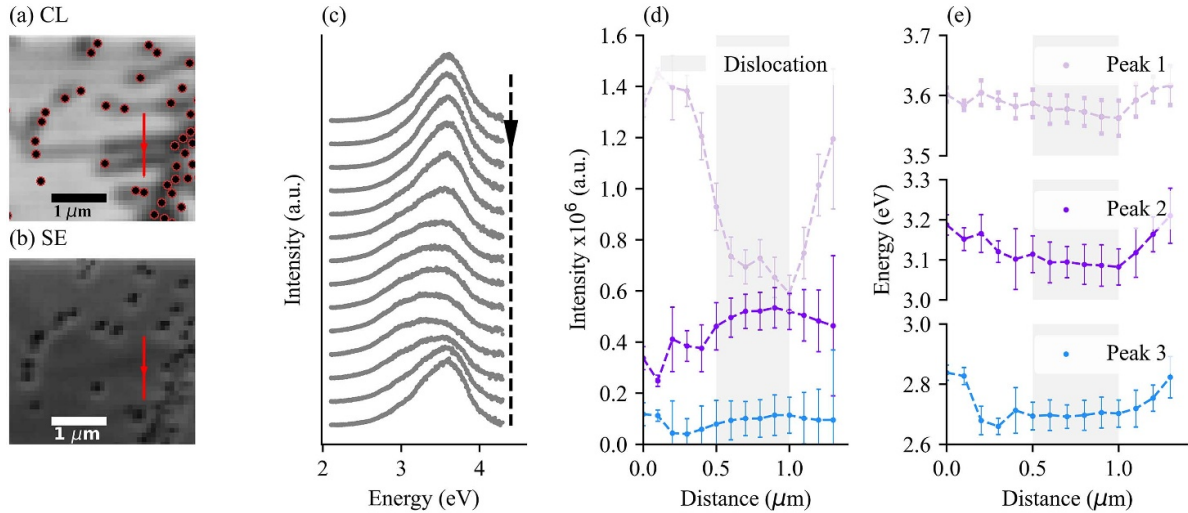
J. Phys. D: Appl. Phys. **58** (2025) 03LT02

▶▶▶ **Letters**

(a) CL
(b) SE
1 μm
1 μm

(c)

(d) Dislocation

(e) Peak 1
Peak 2
Peak 3

Figure 2. Analysis of a linescan taken across 2 dislocation lines. (a) CL (above 3.25 eV) and (b) SE showing the position of the linescan. Evolution of the (c) CL spectra, (d) integrated intensity, and (e) centre energies of the different Gaussian peaks across the lines scan.

atomic structure of the dislocation core (which could depend on the dislocation type, growth method conditions, *etc.*) supported by theoretical modelling of its electronic structure. We attribute the redshifts of the luminescence to strain variations in the vicinity of the dislocation, as the redshift is consistent with the predicted bandgap energy reduction induced by a small percentage of strain [64].

Peaks 2 and 3, centred at *ca.* 3.2 eV and 2.8 eV, respectively, are also observed to vary across the linescan. Both peaks follow a similar trend, whereby their intensity approximately doubles at the dislocation (consistent with the bright contrast lines seen in figure 1(d)). Since these luminescence lines are normally assigned to donor–acceptor pair transitions [38, 46–50], the increased intensity of Peaks 2 and 3 is a strong sign that point defects segregate at the dislocation. Given the high density of point defects present in current Ga_2O_3 samples, it is not surprising to see an accumulation of point defects near dislocations as a mechanism for partial strain release. As mentioned above, the greater density of donor and acceptor states induced by this point defect segregation can provide a competing recombination pathway for the free electrons in the conduction band, partially explaining the decreased intensity of Peak 1 at the dislocation. Looking at the centre energy of Peaks 2 and 3, we observe that both peaks redshift by *ca.* 0.08 eV and 0.1 eV at the dislocation, respectively. It is difficult to interpret this energy shift as it combines several effects, including a reduction of donor–acceptor separation and a variation of strain. While a greater density of donors and acceptors should result in a blueshift of the luminescence, the impact of strain is impossible to predict at present. Donor–acceptor pair luminescence energy is determined by the bandgap energy as well as the donor and acceptor ionisation energies, which are all strain-dependent. However, the strain dependence of these ionization energies is currently unknown, especially when the

donor–acceptor pair luminescence is not assigned to one particular defect but rather to a library of defects.

Figure 3 shows a linescan performed on an etch pit not connected to a dislocation line, i.e. the second category of etch pits. In figure 3(c), we can see that there is no clear variation of the luminescence spectra across the etch pit, which is confirmed in figures 3(d) and (e) with the plots of the integrated intensities and the centre energies of the peak deconvolution—each individual deconvoluted spectrum from the linescan is shown in the supplementary information (figure S2). This further supports the negligible effect of etching on the luminescence. The lack of variation of the integrated intensity and energy of Peaks 1, 2, and 3 indicates that this second category of etch pits must have a different nature than the etch pits connected to dislocation lines (first category of etch pits) analysed in figure 2. Instead of terminating a dislocation that bends from the window region, this second category of etch pit could relate to a different category of dislocation, such as dislocations that nucleate from the coalescence boundary of the ELOG windows [31]—thus having a different atomic environment than a dislocation that bends from the window region. It could also be that this type of etch pit does not relate to dislocations at all, as Oshima *et al* [33] reported that 1.5% of etch pits were not associated with dislocations [33]. This value does not match the 15% proportion of etch pits we associated with the second category, but we must bear in mind that the pit categorisation was based on the presence of (or lack of) a dark line connecting them in the panchromatic CL image. It is possible that some etch pits were wrongfully associated with the second category because the dislocation line they relate to was bending slightly deeper in the sample than what the interaction volume would probe, thus appearing in the CL images as not connected to any line.
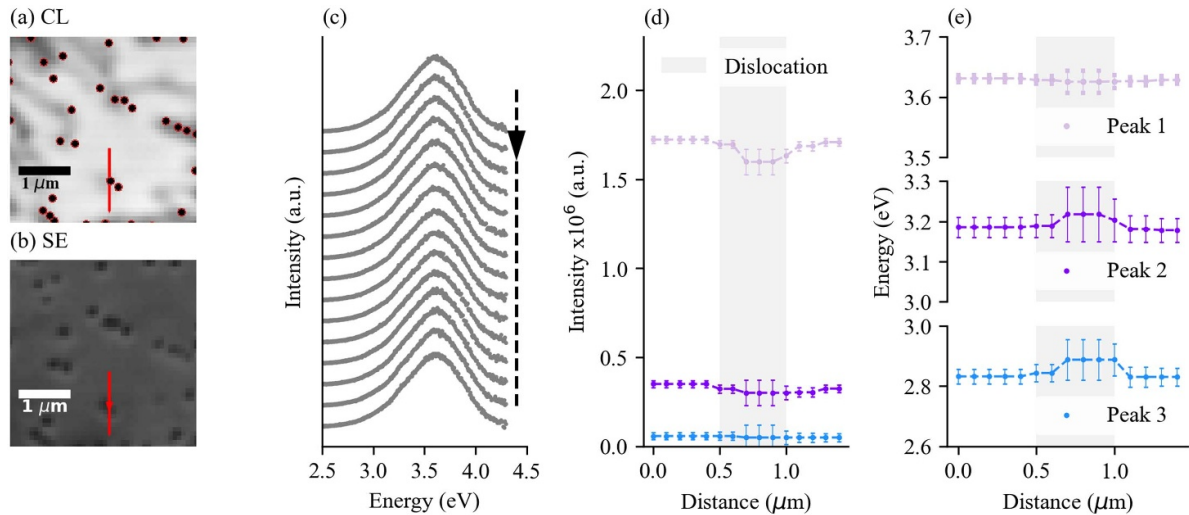
J. Phys. D: Appl. Phys. **58** (2025) 03LT02

▶▶ Letters

Figure 3. Analysis of a linescan taken across an etch pit not connected to a dislocation line. (a) CL (above 3.25 eV) and (b) SE showing the position of the linescan. Evolution of the (c) CL spectra, (d) integrated intensity, and (e) centre energies of the different Gaussian peaks across the lines scan.

4. Conclusion

In conclusion, we conducted the first investigation of the luminescence properties of dislocations in ELOG α-Ga$_2$O$_3$ using CL. The luminescence spectrum at dislocations deviates from that of the regions away from dislocations. We observe a reduction of self-trapped hole-related luminescence (*ca.* 3.6 eV line), which we ascribe to dislocations acting as non-radiative recombination sites for free electrons, to a reduction in free electron density due to Fermi level pinning or to carrier trapping at donor states. An increase in the intensity of the *ca.* 3.2 eV and 2.8 eV lines is also observed, which suggests an increase in the rate of donor–acceptor pair transitions and stands as strong evidence that point defects segregate at dislocations.

Data availability statement

The data that support the findings of this study are openly available from the University of Strathclyde KnowledgeBase at (https://doi.org/10.15129/8bf33f6a-66d1-4a37-9330-422ad03aa382).

ORCID iDs

Mugove Maruzane ⬤ https://orcid.org/0009-0004-9207-0424
Yuichi Oshima ⬤ https://orcid.org/0000-0001-8293-4891
Olha Makydonska ⬤ https://orcid.org/0009-0008-5562-2137
Paul R Edwards ⬤ https://orcid.org/0000-0001-7671-7698
Robert W Martin ⬤ https://orcid.org/0000-0002-6119-764X
Fabien C-P Massabuau ⬤ https://orcid.org/0000-0003-1008-1652

References

[1] Johnson E 1965 Physical limitations on frequency and power parameters of transistors *IRE Int. Conven. Rec.* **13** 27–34
[2] Baliga B J 1989 Power semiconductor device figure of merit for high-frequency applications *IEEE Electron Device Lett.* **10** 455–7
[3] Roy R, Hill V and Osborn E 1952 Polymorphism of Ga$_2$O$_3$ and the system Ga$_2$O$_3$—H$_2$O *J. Am. Chem. Soc.* **74** 719–22
[4] Cora I, Mezzadri F, Boschi F, Bosi M, Čaplovičová M, Calestani G, Dódony I, Pécz B and Fornari R 2017 The real structure of ε-Ga$_2$O$_3$ and its relation to κ-phase *CrystEngComm* **19** 1509–16
[5] Shinohara D and Fujita S 2008 Heteroepitaxy of corundum-structured α-Ga$_2$O$_3$ thin films on α-Al$_2$O$_3$ substrates by ultrasonic mist chemical vapor deposition *Jpn. J. Appl. Phys.* **47** 7311
[6] Roberts J, Chalker P, Ding B, Oliver R, Gibbon J, Jones L, Dhanak V, Phillips L, Major J and Massabuau F-P 2019 Low temperature growth and optical properties of α-Ga$_2$O$_3$ deposited on sapphire by plasma enhanced atomic layer deposition *J. Cryst. Growth* **528** 125254
[7] Kaneko K, Nomura T and Fujita S 2010 Corundum-structured α-phase Ga$_2$O$_3$-Cr$_2$O$_3$-Fe$_2$O$_3$ alloy system for novel functions *Phys. Status Solidi* C **7** 2467–70
[8] Suzuki N, Kaneko K and Fujita S 2014 Growth of corundum-structured (In$_x$Ga$_{1-x}$)$_2$O$_3$ alloy thin films on sapphire substrates with buffer layers *J. Cryst. Growth* **401** 670–2
[9] Jinno R, Chang C S, Onuma T, Cho Y, Ho S-T, Rowe D, Cao M C, Lee K, Protasenko V and Schlom D G *et al* 2021 Crystal orientation dictated epitaxy of ultrawide-bandgap 5.4-to 8.6-eV α-(AlGa)$_2$O$_3$ on m-plane sapphire *Sci. Adv.* **7** eabd5891
[10] Dang G, Yasuoka T, Tagashira Y, Tadokoro T, Theiss W and Kawaharamura T 2018 Bandgap engineering of

α-(Al$_x$Ga$_{1-x}$)$_2$O$_3$ by a mist chemical vapor deposition two-chamber system and verification of Vegard's Law *Appl. Phys. Lett.* **113** 062102

[11] Barthel A, Roberts J, Napari M, Frentrup M, Huq T, Kovács A, Oliver R, Chalker P, Sajavaara T and Massabuau F 2020 Ti alloyed α-Ga$_2$O$_3$: route towards wide band gap engineering *Micromachines* **11** 1128

[12] Williams M S, Alonso-Orts M, Schowalter M, Karg A, Raghuvansy S, McCandless J P, Jena D, Rosenauer A, Eickhoff M and Vogt P 2024 Growth, catalysis and faceting of α-Ga$_2$O$_3$ and α-(In$_x$Ga$_{1-x}$)$_2$O$_3$ on m-plane α-Al$_2$O$_3$ by molecular beam epitaxy *APL Mater.* **12** 011120

[13] Oshima Y, Víllora E G and Shimamura K 2015 Halide vapor phase epitaxy of twin-free α-Ga$_2$O$_3$ on sapphire (0001) substrates *Appl. Phys. Express* **8** 055501

[14] Yao Y, Okur S, Lyle L A, Tompa G S, Salagaj T, Sbrockey N, Davis R F and Porter L M 2018 Growth and characterization of α-, β- and ϵ-phases of Ga$_2$O$_3$ using MOCVD and HVPE techniques *Mater. Res. Lett.* **6** 268–75

[15] Son H and Jeon D-W 2019 Optimization of the growth temperature of α-Ga$_2$O$_3$ epilayers grown by halide vapor phase epitaxy *J. Alloys Compd.* **773** 631–5

[16] Oshima T, Okuno T and Fujita S 2007 Ga$_2$O$_3$ thin film growth on c-plane sapphire substrates by molecular beam epitaxy for deep-ultraviolet photodetectors *Jpn. J. Appl. Phys.* **46** 7217

[17] Schewski R, Wagner G, Baldini M, Gogova D, Galazka Z, Schulz T, Remmele T, Markurt T, Von Wenckstern H and Grundmann M *et al* 2014 Epitaxial stabilization of pseudomorphic α-Ga$_2$O$_3$ on sapphire (0001) *Appl. Phys. Express* **8** 011101

[18] Guo D, Zhao X, Zhi Y, Cui W, Huang Y, An Y, Li P, Wu Z and Tang W 2016 Epitaxial growth and solar-blind photoelectric properties of corundum-structured α-Ga$_2$O$_3$ thin films *Mater. Lett.* **164** 364–7

[19] Cheng Z, Hanke M, Vogt P, Bierwagen O and Trampert A 2017 Phase formation and strain relaxation of Ga$_2$O$_3$ on c-plane and a-plane sapphire substrates as studied by synchrotron-based x-ray diffraction *Appl. Phys. Lett.* **111** 162104

[20] Sun H, Li K-H, Castanedo C T, Okur S, Tompa G S, Salagaj T, Lopatin S, Genovese A and Li X 2018 HCl flow-induced phase change of α-, β- and ε-Ga$_2$O$_3$ films grown by MOCVD *Cryst. Growth Des.* **18** 2370–6

[21] Ma T, Chen X, Ren F, Zhu S, Gu S, Zhang R, Zheng Y and Ye J 2019 Heteroepitaxial growth of thick α-Ga$_2$O$_3$ film on sapphire (0001) by MIST-CVD technique *J. Semiconduct.* **40** 012804

[22] Hao J, Ma T, Chen X, Kuang Y, Li L, Li J, Ren F-F, Gu S, Tan H H and Jagadish C *et al* 2020 Phase tailoring and wafer-scale uniform hetero-epitaxy of metastable-phased corundum α-Ga$_2$O$_3$ on sapphire *Appl. Surf. Sci.* **513** 145871

[23] Roberts J, Jarman J, Johnstone D, Midgley P, Chalker P, Oliver R and Massabuau F-P 2018 α-Ga$_2$O$_3$ grown by low temperature atomic layer deposition on sapphire *J. Cryst. Growth* **487** 23–27

[24] Wheeler V D *et al* 2020 Phase control of crystalline Ga$_2$O$_3$ films by plasma-enhanced atomic layer deposition *Chem. Mater.* **32** 1140–52

[25] Kasu M, Hanada K, Moribayashi T, Hashiguchi A, Oshima T, Oishi T, Koshi K, Sasaki K, Kuramata A and Ueda O 2016 Relationship between crystal defects and leakage current in β-Ga$_2$O$_3$ Schottky barrier diodes *Jpn. J. Appl. Phys.* **55** 1202BB

[26] Yang J, Fares C, Elhassani R, Xian M, Ren F, Pearton S, Tadjer M and Kuramata A 2019 Reverse breakdown in large area, field-plated, vertical β-Ga$_2$O$_3$ rectifiers *ECS J. Solid State Sci. Technol.* **8** Q3159

[27] Akaiwa K, Ota K, Sekiyama T, Abe T, Shinohe T and Ichino K 2020 Electrical Properties of Sn-Doped α-Ga$_2$O$_3$ Films on m-Plane Sapphire Substrates Grown by Mist Chemical Vapor Deposition *Phys. Status Solidi* a **217** 1900632

[28] Takane H, Izumi H, Hojo H, Wakamatsu T, Tanaka K and Kaneko K 2023 Effect of dislocations and impurities on carrier transport in α-Ga$_2$O$_3$ on m-plane sapphire substrate *J. Mater. Res.* **38** 2645–54

[29] Oshima Y, Kawara K, Shinohe T, Hitora T, Kasu M and Fujita S 2019 Epitaxial lateral overgrowth of α-Ga$_2$O$_3$ by halide vapor phase epitaxy *APL Mater.* **7** 022503

[30] Son H, Choi Y-J, Ha J-S, Jung S H and Jeon D-W 2019 Crystal quality improvement of α-Ga$_2$O$_3$ growth on stripe patterned template via epitaxial lateral overgrowth *Cryst. Growth Des.* **19** 5105–10

[31] Kawara K, Oshima T, Okigawa M and Shinohe T 2020 In-plane anisotropy in the direction of the dislocation bending in α-Ga$_2$O$_3$ grown by epitaxial lateral overgrowth *Appl. Phys. Express* **13** 115502

[32] Kawara K, Oshima Y, Okigawa M and Shinohe T 2020 Elimination of threading dislocations in α-Ga$_2$O$_3$ by double-layered epitaxial lateral overgrowth *Appl. Phys. Express* **13** 075507

[33] Oshima Y, Yagyu S and Shinohe T 2021 Visualization of threading dislocations in an α-Ga$_2$O$_3$ epilayer by HCl gas etching *J. Cryst. Growth* **576** 126387

[34] Edwards P R and Martin R W 2011 Cathodoluminescence nano-characterization of semiconductors *Semicond. Sci. Technol.* **26** 064005

[35] Massabuau F C, Rhode S L, Horton M K, O'Hanlon T J, Kovács A, Zielinski M S, Kappers M J, Dunin-Borkowski R E, Humphreys C J and Oliver R A 2017 Dislocations in AlGaN: core structure, atom segregation and optical properties *Nano Lett.* **17** 4846–52

[36] Naresh-Kumar G, Bruckbauer J, Edwards P R, Kraeusel S, Hourahine B, Martin R W, Kappers M J, Moram M A, Lovelock S and Oliver R A *et al* 2014 Coincident electron channeling and cathodoluminescence studies of threading dislocations in GaN *Microsc. Microanal.* **20** 55–60

[37] Kaganer V, Lahnemann J, Pfuller C, Sabelfeld K, Kireeva A and Brandt O 2019 Determination of the Carrier Diffusion Length in GaN from Cathodoluminescence Maps Around Threading Dislocations: Fallacies and Opportunities *Phys. Rev. Appl.* **12** 054038

[38] Harwig T and Kellendonk F 1978 Some observations on the photoluminescence of doped β-galliumsesquioxide *J. Solid State Chem.* **24** 255–63

[39] Onuma T, Nakata Y, Sasaki K, Masui T, Yamaguchi T, Honda T, Kuramata A, Yamakoshi S and Higashiwaki M 2018 Modeling and interpretation of UV and blue luminescence intensity in β-Ga$_2$O$_3$ by silicon and nitrogen doping *J. Appl. Phys.* **124** 075103

[40] Shimamura K, Víllora E G, Ujiie T and Aoki K 2008 Excitation and photoluminescence of pure and Si-doped β-Ga$_2$O$_3$ single crystals *Appl. Phys. Lett.* **92** 201914

[41] Nicol D, Oshima Y, Roberts J, Penman L, Cameron D, Chalker P, Martin R and Massabuau F-P 2023 Hydrogen-related 3.8 eV UV luminescence in α-Ga$_2$O$_3$ *Appl. Phys. Lett.* **122** 062102

[42] Moriya R, Kikawa J, Mouri S, Shinohe T, Xiao S, Miyake H and Araki T 2022 Cathodoluminescence Study of m-Plane α-Ga$_2$O$_3$ Grown by Mist Chemical Vapor Deposition *Phys. Status Solidi* b **259** 2100598

[43] Ghadbeigi L, Cooke J, Dang G T, Kawaharamura T, Yasuoka T, Sun R, Ranga P, Krishnamoorthy S, Scarpulla M A and Sensale-Rodriguez B 2021 Optical characterization of gallium oxide α and β polymorph thin-films grown on c-plane sapphire *J. Electron. Mater.* **50** 2990–8

[44] Hou Y, Wu L, Wang X, Ding Z, Li Z and Fu X 2007 Photocatalytic performance of α-, β- and γ-Ga_2O_3 for the destruction of volatile aromatic pollutants in air *J. Catal.* **250** 12–18

[45] Frodason Y K, Johansen K, Vines L and Varley J 2020 Self-trapped hole and impurity-related broad luminescence in β-Ga_2O_3 *J. Appl. Phys.* **127** 075701

[46] Cho S, Lee J, Park I Y and Kim S 2002 Temperature dependence of photoluminescence of α-Ga_2O_3 powders *Jpn. J. Appl. Phys.* **41** 5237

[47] Onuma T, Fujioka S, Yamaguchi T, Higashiwaki M, Sasaki K, Masui T and Honda T 2013 Correlation between blue luminescence intensity and resistivity in β-Ga_2O_3 single crystals *Appl. Phys. Lett.* **103** 041910

[48] Binet L and Gourier D 1998 Origin of the blue luminescence of β-Ga_2O_3 *J. Phys. Chem. Solids* **59** 1241–9

[49] Herbert W C, Minnier H B and Brown J J 1969 Self-Activated Luminescence of β-Ga_2O_3 *J. Electrochem. Soc.* **116** 1019

[50] Varley J B, Weber J R, Janotti A and Van de Walle C G 2010 Oxygen vacancies and donor impurities in β-Ga_2O_3 *Appl. Phys. Lett.* **97** 142106

[51] Wakai H, Sinya Y and Yamanaka A 2011 Effect of $Cr3+$ ions on optical properties in β-Ga_2O_3 semiconductor *Phys. Status Solidi* c **8** 537–9

[52] Nie Y, Jiao S, Li S, Lu H, Liu S, Yang S, Wang D, Gao S, Wang J and Li Y 2022 Modulating the blue and green luminescence in the β-Ga_2O_3 films *J. Alloys Compd.* **900** 163431

[53] Naresh-Kumar G, MacIntyre H, Subashchandran S, Edwards P R, Martin R W, Daivasigamani K, Sasaki K and Kuramata A 2021 Origin of Red Emission in β-Ga_2O_3 Analyzed by Cathodoluminescence and Photoluminescence Spectroscopy *Phys. Status Solidi* b **258** 2000465

[54] Song Y, Zhang H, Lin C, Zhu Y, Li G, Yang F and Yu D 2004 Luminescence emission originating from nitrogen doping of β-Ga_2O_3 nanowires *Phys. Rev. B* **69** 075304

[55] Chang L-W, Lu T-Y, Chen Y-L, Yeh J-W and Shih H C 2011 Effect of the doped nitrogen on the optical properties of β-Ga_2O_3 nanowires *Mater. Lett.* **65** 2281–3

[56] Pozina G, Forsberg M, Kaliteevski M and Hemmingsson C 2017 Emission properties of Ga_2O_3 nano-flakes: Effect of excitation density *Sci. Rep.* **7** 42132

[57] Cooke J, Ranga P, Jesenovec J, McCloy J S, Krishnamoorthy S, Scarpulla M A and Sensale-Rodriguez B 2022 Effect of extended defects on photoluminescence of gallium oxide and aluminum gallium oxide epitaxial films *Sci. Rep.* **12** 3243

[58] Drouin D, Couture A R, Joly D, Tastet X, Aimez V and Gauvin R 2007 CASINO V2. 42—a fast and easy-to-use modeling tool for scanning electron microscopy and microanalysis users *Scanning* **29** 92–101

[59] Brenny B, Coenen T and Polman A 2014 Quantifying coherent and incoherent cathodoluminescence in semiconductors and metals *J. Appl. Phys.* **115** 244307

[60] Varley J B, Janotti A, Franchini C and Van de Walle C G 2012 Role of self-trapping in luminescence and p-type conductivity of wide-band-gap oxides *Phys. Rev. B* **85** 081109

[61] Brantley W, Lorimor O, Dapkus P, Haszko S and Saul R 1975 Effect of dislocations on green electroluminescence efficiency in GaP grown by liquid phase epitaxy *J. Appl. Phys.* **46** 2629–37

[62] Herzog A, Keune D and Craford M 1972 High-Efficiency Zn-Diffused GaAs Electroluminescent Diodes *J. Appl. Phys.* **43** 600–8

[63] Cherns D and Jiao C 2001 Electron holography studies of the charge on dislocations in GaN *Phys. Rev. Lett.* **87** 205504

[64] Kawamura T and Akiyama T 2022 Bandgap engineering of α-Ga_2O_3 by hydrostatic, uniaxial and equibiaxial strain *Jpn. J. Appl. Phys.* **61** 021005